Local strain exerted on Nb_3Sn filaments in an ITER strand

2015 Supercond. Sci. Technol. 28 045016

(http://iopscience.iop.org/0953-2048/28/4/045016)

IOP Publishing Superconductor Science and Technology
Supercond. Sci. Technol. **28** (2015) 045016 (9pp) doi:10.1088/0953-2048/28/4/045016

Local strain exerted on Nb_3Sn filaments in an ITER strand

Kozo Osamura[1], Shutaro Machiya[2], Stefanus Harjo[3], Tatsushi Nakamoto[4], Najib Cheggour[5,6] and Arend Nijhuis[7]

[1] Research Institute for Applied Sciences, Tanaka Ohi-cho 49, Sakyo-ku, Kyoto 606-8202, Japan
[2] Department of Mechanical Engineering, Daido University, Takiharu, Minami-ku, Nagoya, Aichi 457-8530, Japan
[3] J-PARC Center, Japan Atomic Energy Agency, 2-4 Shirane Shirakata, Tokai-mura, Naka-gun, Ibaraki 319-1195, Japan
[4] Cryogenics Science Center, High Energy Accelerator Research Organization (KEK) 1-1 Oho, Tsukuba, Ibaraki, 305-0801, Japan
[5] Electromagnetics Division, National Institute of Standards and Technology, Boulder, CO 80305, USA
[6] Department of Physics, University of Colorado, Boulder, CO 80309, USA
[7] Energy, Materials and Systems, University of Twente, 7500 AE Enschede, The Netherlands

E-mail: kozo_osamura@rias.or.jp

Received 30 October 2014
Accepted for publication 31 January 2015
Published 13 March 2015

Abstract

As part of an international project to benchmark facilities for measuring the strain dependence of critical current in International Thermonuclear Experimental Reactor (ITER) Nb_3Sn strands, direct measurement of local strain exerted on Nb_3Sn filaments was attempted at cryogenic temperature by means of a pulsed neutron technique. The lattice axial strain increased linearly with a slope close to unity against applied strain, while the thermal axial strain was −0.22% at 8.5 K. As a result, the force-free strain was evaluated to be 0.22–0.23%. This key parameter should provide an accurate estimate of the peak location of critical current versus applied strain. The lattice transverse strain decreased linearly as a function of applied strain with a slope of 0.33–0.34. The lattice strains of the Nb and Cu components were also measured and their behavior was analyzed by computing diffraction elastic moduli based on micromechanics theories. The stress–strain curve calculated according to the rule of mixtures described quite well the macroscopic curve measured for the present ITER Nb_3Sn strand.

Keywords: superconductor, Nb_3Sn, residual strain, ITER, neutron diffraction, diffraction elastic modulus, micromechanics

(Some figures may appear in colour only in the online journal)

1. Introduction

Strain sensitivity of critical current I_c in Nb_3Sn composite superconducting strands has been studied by many investigators from both physical and practical viewpoints. According to recent theories [1–5], the position of the maximum I_c in the strain dependency curve has been predicted to be at the point where the three-dimensional deviatoric strain components relating to the anharmonic terms of lattice vibrations are minimal. It is highly desirable to verify experimentally these theoretical predictions. The only tool to measure non-invasively the local strain exerted on the superconducting component in a composite wire is the quantum beam technique [6]. Recently, we reported preliminary results on the local strain of Nb_3Sn filaments in an International Thermonuclear Experimental Reactor (ITER) strand and discussed the coincidence with theoretical predictions [7].

Test methods to measure the strain dependence of I_c are not yet standardized. Several strain measurement facilities have been developed world-wide to enable in-depth studies of the strain effect. Measurement techniques for investigating the effect of axial strain along the strand are classified in two

categories [8]. The first category is characterized by the method where the sample can freely shrink during cooling down. It allows determining directly the natural pre-compressive strain of the sample. The second category, where the sample is soldered onto a thick ring called a Pacman or onto a multi-turn spring device called a Walters spring, does not allow for a direct determination of the pre-compressive strain, but offers vast possibilities for studying the effect of both tensile and compressive axial strain [8].

Despite the diversity in the techniques, very little has been done to directly compare the results obtained by these apparatuses for cross benchmarking. Recently an inter-laboratory comparison test has been proposed [9] in order to compare critical-current data obtained as a function of strain on the same wire by various apparatuses. One key point is to know exactly the local strain exerted on Nb_3Sn filaments when an external stress is applied to the Nb_3Sn benchmarking strand by use of the various measurement methods mentioned above. The local strain consists of thermal and lattice strains. The latter is strain induced by externally applied stress. In practice, the local strain is not equal to the applied strain because the local strain is affected by the thermal strain and anisotropy of the elastic moduli. Thus the modern quantum beam technique is quite unique for investigating accurately the strain state of Nb_3Sn filaments in the composite strand.

In conjunction with the international program for strain benchmarking tests, the present mission is to measure exactly the local strain exerted on Nb_3Sn filaments under various strain conditions. Pulsed neutrons were utilized for getting information along both the axial and transverse directions and for getting multi-diffractions from all constituent components. Diffraction data allowed evaluation of the local strain exerted on all constituent components as a function of applied strain. The behavior of local strains was analyzed on the basis of micromechanics.

2. Experimental method

The Nb_3Sn strand examined herein was from the same wire that was used for the strain benchmarking experiment [9]. It consists of 11 000 superconductor filaments embedded in a bronze matrix and surrounded by a Nb barrier and Cu stabilizer. The original composition of bronze was 15.5 wt% Sn–0.3 wt% Ti. The constituents of a similar Nb_3Sn strand fabricated by the same Japanese manufacturer are listed in the appendix. According to preliminary electron microscope analysis, the Sn concentration of the Cu–Sn matrix was 0.9–1.1 wt% Sn after the reaction heat treatment. This low Sn concentration suggested that the matrix is in the state of α primary solid solution and its mechanical properties should be close to that of pure Cu.

Neutron diffraction measurements were carried out at the beam line BL19 TAKUMI of Japan Proton Accelerator Research Complex (J-PARC), where pulsed neutrons with wavelengths between 0.06 and 0.2 nm were utilized [6]. The diffracted beams were investigated by means of two detector banks consisting of ^{3}He detectors, which were placed at two

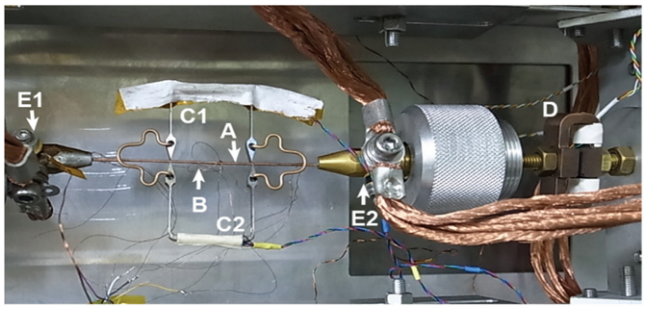

Figure 1. Set-up for the diffraction experiment, where (A): single Nb_3Sn strand; (B): strain gage; (C1), (C2): Nyilas type extensometer; (D): load cell; and (E1), (E2): temperature sensor.

Figure 2. Sample holder for diffraction measurements as a function of temperature. (A)–(F) are slots for samples and (T1), (T2) are temperature sensors.

positions orthogonal to the incident beam. The southern data bank accumulated the diffracted neutrons with scattering vector parallel to the strand axis, while the northern one accumulated the diffracted neutrons transverse to the strand axis. In principle, each data bank was able to accumulate two dimensional data with respect to the wavelength and diffraction angle.

A specially designed load frame [10] was used in the present simultaneous tensile test and diffraction experiment. The load frame was placed at the center of a goniometer. As shown in figure 1, the single wire sample was gripped by brass chucks. A Nyilas-type extensometer marked by C2 in figure 1 was attached to the sample to measure *applied strain A*. The applied strain was also measured with three strain gages (B) glued on the wire sample. Load was measured with

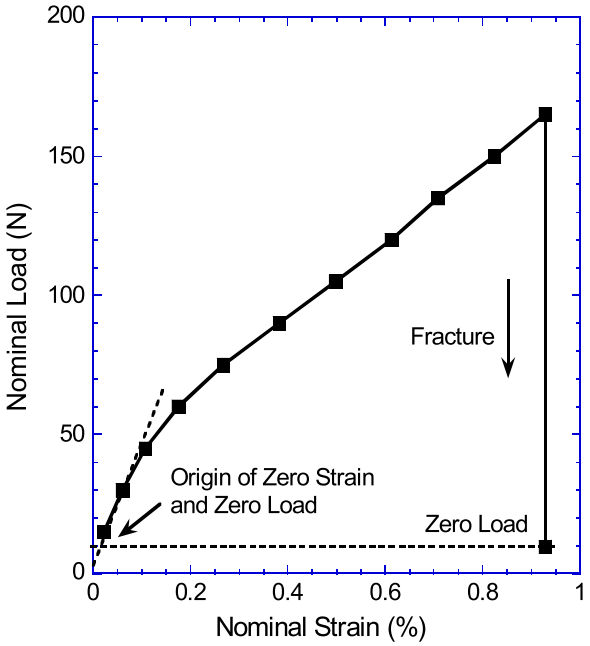

Figure 3. Determination of the origin for the load and strain curve.

a load cell indicated by D in figure 1. The sample was loaded to successive constant load level *step by step*.

Diffraction measurements were also conducted as a function of temperature to study thermal strain. The sample holder shown in figure 2 was attached directly to the cold head of a Gifford-McMahon refrigerator. The sample was inserted in one of the six slots (A–F) available on the holder.

3. Experimental result

3.1. Load and strain relation

A difficulty of the experiment at cryogenic temperatures originated from thermally induced instabilities due to excess load on the sample during cooling. It was not possible to initialize the tensile test condition so the applied load on the sample was zero. Therefore, we estimated the zero-load and zero-strain origin as follows (see figure 3): the load was increased to fracture the sample and the nominal load after fracture was recorded as indicated by 'zero-load' in figure 3. The point corresponding to 'zero-load' on the measured load versus strain curve was defined as the origin of zero-strain and zero-load.

Figure 4 depicts the stress (R) versus strain (A) curve measured at 8.5 K for the Nb_3Sn strand, where open circles indicate the experimental data. It shows a typical elasto-plastic behavior. The solid curve indicated as RKroener is a fit to the result calculated by use of the Kroener model as described later in section 4.4.

3.2. Diffraction experiment

Figure 5 shows the intensity profile as a function of time of flight along the transverse direction of the Nb_3Sn sample.

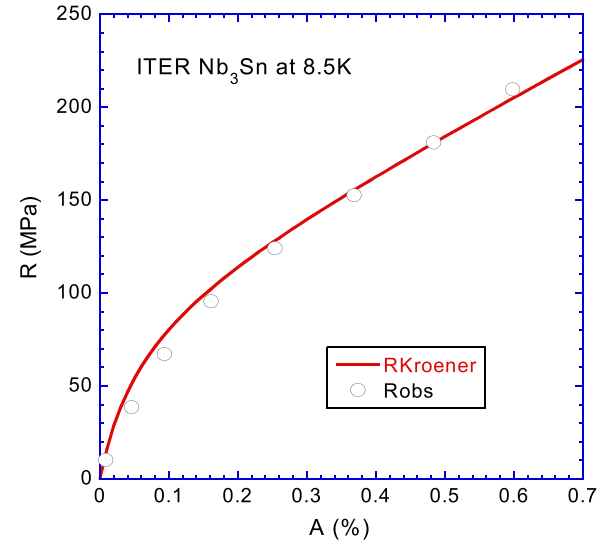

Figure 4. Stress versus strain curve at 8.5 K for the Nb_3Sn strand.

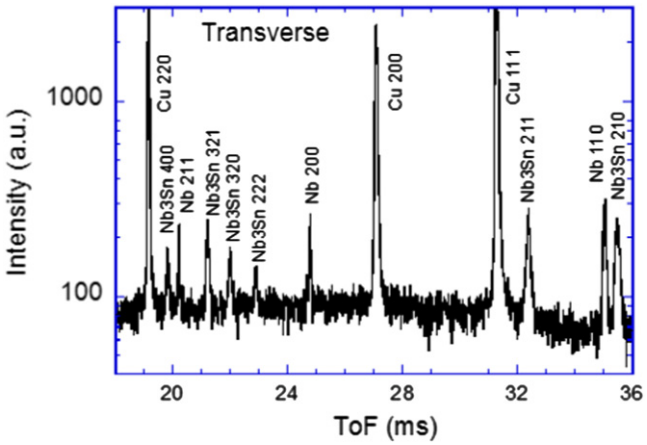

Figure 5. Intensity profile as a function of time of flight along the transverse direction of the Nb_3Sn sample.

Several diffraction peaks for Nb_3Sn, Nb and Cu were observed. The Cu peaks consist of peaks from pure Cu and Cu–Sn solid solution. They were treated as a single peak because their half width was almost the same the other peaks. In the present analysis, the following diffraction peaks were utilized: (210), (211) and (321) for Nb_3Sn, (110), (200) and (211) for Nb and (111), (200) and (220) for Cu components.

3.2.1. Thermal strain. It is important to know the local strain exerted on Nb_3Sn filaments in order to properly investigate its effect on I_c. Measurement of thermal strain was carried out at 8.5 K and room temperature. In order to know the crystal plane spacing at the strain-free state, Nb_3Sn filaments were extracted from the same wire sample by dissolving the copper and bronze in nitric acid. Filament fragments were placed inside an aluminum tube and inserted in one of the slots shown in figure 2. The crystal plane spacing of Nb_3Sn in the free filaments $d^{pT}_{Nb_3Sn}$ was defined as the strain-free plane

Table 1. Thermal strains exerted on Nb_3Sn filaments along the axial and transverse directions at 8.5 K and room temperature.

	8.5 K		RT	
hkl	$A^T_{Nb_3Sn}$(axial) (%)	$A^T_{Nb_3Sn}$(transv) (%)	$A^T_{Nb_3Sn}$(axial) (%)	$A^T_{Nb_3Sn}$(transv) (%)
210	(−0.26)	(0.025)	(−0.14)	(0.010)
211	−0.23	0.045	−0.11	0.017
321	−0.21	0.042	−0.11	0.019
Average	−0.22	0.043	−0.11	0.018

spacing measured at temperature T. Also, a Nb_3Sn wire sample was cut into small pieces and placed in a second aluminum tube and inserted in a different slot in the diffraction-measurement sample holder. The *thermal strain* is given by

$$A^T_{Nb_3Sn} = \frac{\left[d(0)^T_{Nb_3Sn} - d^{pT}_{Nb_3Sn}\right]}{d^{pT}_{Nb_3Sn}} 100\,(\%), \qquad (1)$$

where $d(0)^T_{Nb_3Sn}$ is the crystal plane spacing of Nb_3Sn in the wire measured at temperature T. Thermal strain was evaluated from three diffraction peaks (table 1). The (210) data was different from (211) and (321) data, which difference was attributed to the influence of the strong (111) peak of aluminum tube close to the (210) peak of Nb_3Sn. So, data from (210) peaks were not considered to evaluate the thermal strain. The averaged thermal strain using two (210) and (321) data was adopted in the present analysis. On the other hand, in the simultaneous tensile test and diffraction experiment that used the tensile jig as shown in figure 1, the (210) diffraction was not influenced by the (111) peak of aluminum, because the aluminum tube was not used.

Thermal strain data at temperature T listed in table 1 indicate the strain accumulated during sample cooling after the heat treatment for reacting Nb_3Sn compound.

3.2.2. Lattice strain. When strain is applied by the load frame as shown in figure 1, Nb_3Sn filaments elongate and the crystal plane spacing changes from $d(0)^T_{Nb_3Sn}$ to $d(A)^T_{Nb_3Sn}$. The *lattice strain* is defined as

$$A^{latticeT}_{Nb_3Sn}(A) = \frac{d(A)^T_{Nb_3Sn} - d(0)^T_{Nb_3Sn}}{d^{pT}_{Nb_3Sn}} \cdot 100(\%) \qquad (2)$$

Figure 6 shows the dependence on applied strain of the lattice strain along the wire axis at 8.5 K. This dependence evaluated from three diffraction peaks looks nearly the same. The straight lines are linear-regression analyses of the data and the resulting slopes are listed in table 2.

Figure 7 shows the dependence on applied strain of the lattice strain transverse to the strand axis at 8.5 K. The straight lines are linear-regression analyses of the data. Their respective slopes are listed in table 2.

As seen in figures 6 and 7, the magnitude of the slope for (210) diffraction is smaller than the others. This phenomenon is attributed to differences in the diffraction elastic modulus depending on the crystal orientation. The slope is inversely

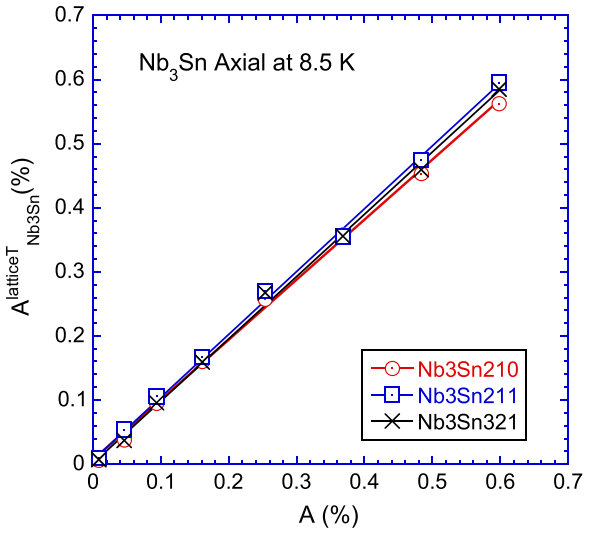

Figure 6. Lattice strain at 8.5 K on Nb_3Sn filaments along the strand axis as a function of applied strain.

Table 2. Slope for the Nb_3Sn lattice strain on filaments versus applied strain curves at 8.5 K.

hkl	Slope (axial)	Slope (transverse)	Poisson ratio
210	0.94	−0.33	0.35
211	0.98	−0.34	0.34
321	0.97	−0.34	0.35

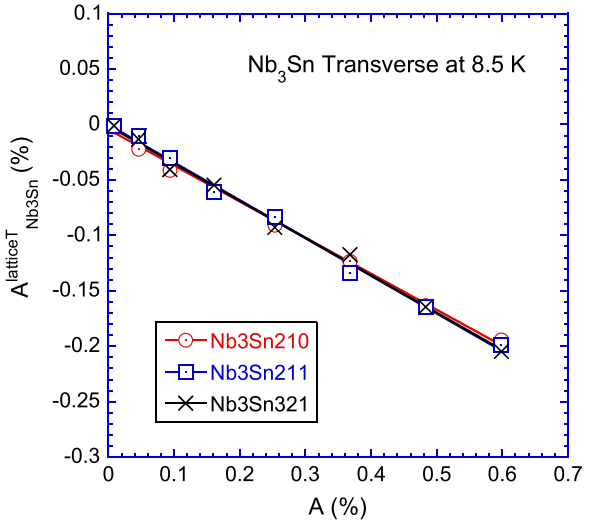

Figure 7. Lattice strain at 8.5 K on Nb_3Sn filaments transverse to the strand axis as a function of applied strain.

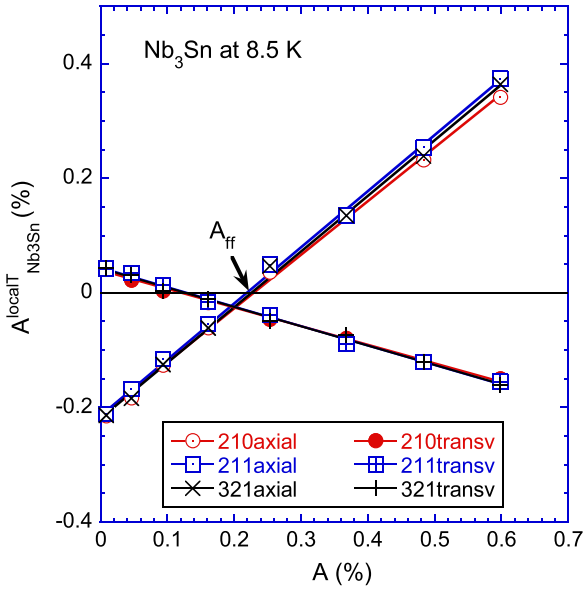

Figure 8. Local strain exerted on Nb_3Sn filaments at 8.5 K as a function of applied strain.

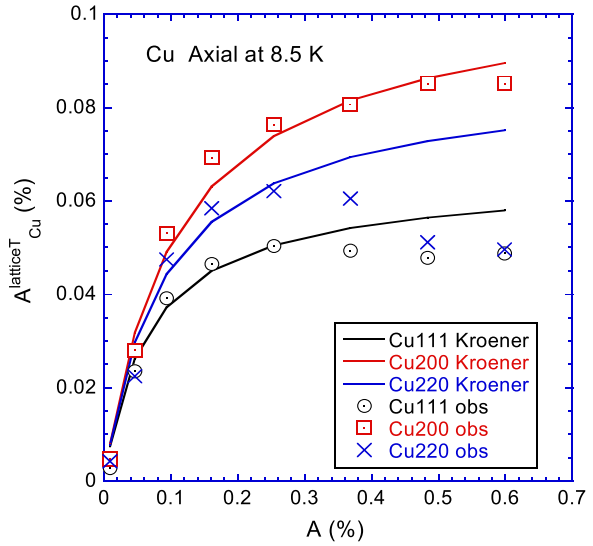

Figure 9. Lattice strain at 8.5 K exerted on the Cu component along the strand axis as a function of applied strain, where 'obs' and 'Kroener' indicate experimental and theoretical data, respectively.

proportional to the diffraction elastic modulus as will be discussed later.

3.2.3. Local strain. The *local strain* exerted on the Nb_3Sn filaments is given by the sum of the lattice and thermal strains as follows:

$$A^{\text{local}T}_{\text{Nb}_3\text{Sn}}(A) = A^{T}_{\text{Nb}_3\text{Sn}} + A^{\text{lattice}T}_{\text{Nb}_3\text{Sn}}(A). \quad (3)$$

We used the average values of thermal strains along the axial and transverse directions (listed in table 1) to calculate the local strain. Results are depicted in figure 8. We define the force free strain A_{ff} as the applied strain where the local stress exerted on Nb_3Sn filaments becomes zero along the axial direction (even though it is not zero in the transverse direction). A_{ff} was approximately 0.22–0.23% applied strain at 8.5 K.

3.2.4. Lattice strain exerted on Cu and Cu–Sn. As mentioned above, it was not possible to separate two diffraction peaks for the Cu and Cu–Sn components. They were presumed to be a single diffraction peak and are called the 'Cu component'. Figure 9 shows the dependence of the Cu component's lattice strain on applied strain, where lattice strain was evaluated from the (111), (200) and (220) diffraction peaks. This dependence was non-linear and tended to saturate with increasing applied strain. This non-linearity suggests that the Cu component deforms plastically. The solid curves are the results of data fitting described in section 4.4.

The Cu component's lattice strain in the transverse direction is depicted in figure 10 as a function of applied strain and showed a non-linear behavior similar to that along the axial direction.

3.2.5. Lattice strain exerted on Nb. Figure 11 shows the dependence of the Nb lattice strain on applied strain, where

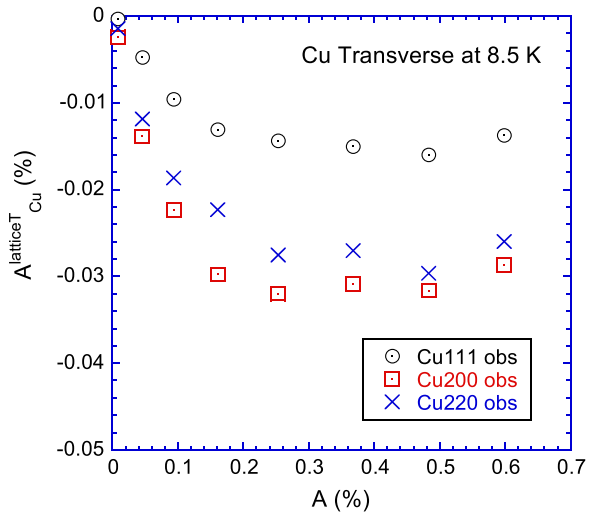

Figure 10. Lattice strain at 8.5 K on the Cu component transverse to the strand axis as a function of applied strain.

the Nb existed in the strand as core and barrier as listed in table A1. Only the major diffraction (110) peak was observed because Nb was well oriented along the axial direction. Nb lattice strain depends linearly on applied strain (slope listed in table 3). The dependence of Nb lattice strain transverse to the strand axis on applied strain is shown in figure 12. The slopes of (200), (211) and (110) were dissimilar. We suggest that slope differences are related to anisotropic diffraction elastic modulus along these crystal orientations.

4. Discussion

4.1. Strain measurement

In the present experiment, strain was measured by use of a Nyilas extensometer (marked by C2 in figure 1) that was

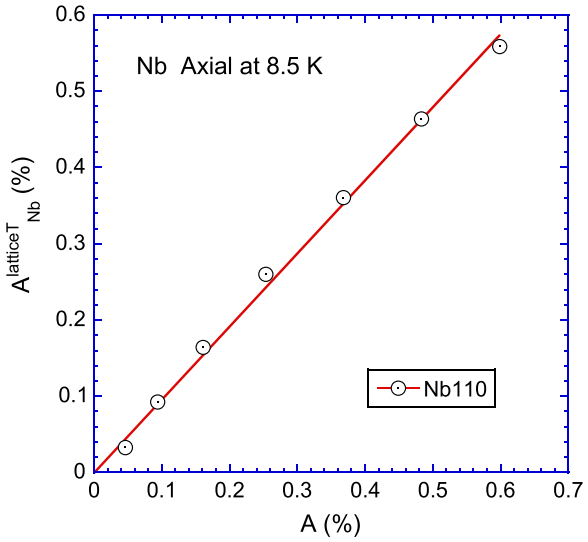

Figure 11. Lattice strain at 8.5 K exerted on Nb along the strand axis as a function of applied strain.

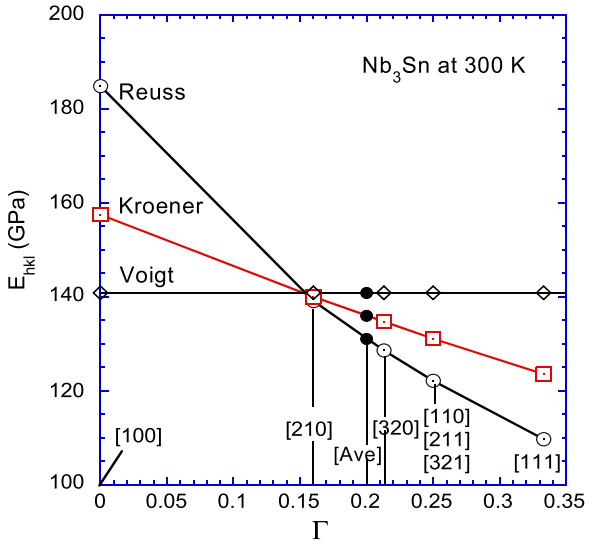

Figure 13. Computational diffraction elastic moduli as a function of direction parameter Γ for Nb_3Sn based on the Reuss, Kroener and Voigt models.

Table 3. Slope obtained from the linear regression analysis of the Nb lattice strain versus applied strain curves at 8.5 K.

hkl	Slope (axial)	Slope (transverse)
110	0.958	−0.487
200	—	−0.236
211	—	−0.351

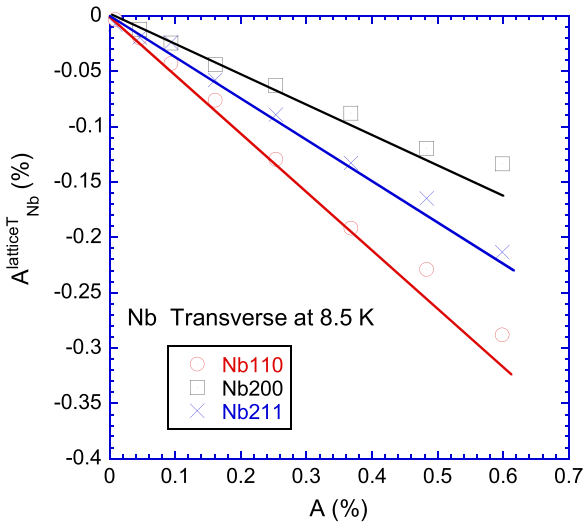

Figure 12. Nb lattice strain at 8.5 K transverse to the strand axis as a function of applied strain.

corrected in terms of temperature compensation. Three strain gages, mounted directly on the wire sample, were also used but only for reference because their temperature compensation factor could not be calibrated. Data from the three strain gages were qualitatively consistent with those measured with the Nyilas extensometer, that is, the ratio of both data became nearly constant, independent of applied stress.

4.2. Influence of strain gages on the mechanical properties

The three strain gages, which were 1.1 mm wide and 1.2 mm long, were glued on the round 0.8 mm diameter strand. One strain gage was on the sample region located within the Nyilas extensometer arms and the other two were outside this region. The inside gage could possibly influence the rigidity of the strand. However the gage length of the sample portion located inside the Nyilas extensometer was 25 mm and, therefore, the area fraction covered by the strain gage was 2.1% only. Furthermore, the modulus of elasticity of polyimide (3–7 GPa), the main component of the strain gage, is very small in comparison to that of Nb_3Sn strand (100 GPa). Thus the influence of the strain gage on the strand's mechanical properties is negligible.

4.3. Diffraction elastic constant

The diffraction elastic constant of a polycrystalline sample is influenced by the grain configuration. When the grains align parallel to the tensile axis, like bamboo, each grain is presumed to be pulled by a uniform stress. Then the elastic constants can be evaluated on the basis of micromechanics according to the Reuss model [11]. On the other extreme, the Voigt model is applicable when grains are under a uniform strain [12]. As an ideal case, homogeneous grain configuration is defined as equiaxed grains distributed randomly where their crystal axis does not orient towards a specific direction. The Kroener model [13] gives a solution for a polycrystalline sample with such a homogeneous grain configuration.

Based on the following compliance constants for Nb_3Sn: $S_{11} = 5.411$, $S_{12} = -1.660$ and $S_{44} = 25.25\ \mathrm{TPa}^{-1}$ at 300 K [14, 15], the diffraction elastic modulus, E_{hkl} was evaluated by use of the above mentioned three models as shown in figure 13, where the direction parameter Γ is given by the

equation,

$$\Gamma = \frac{h^2k^2 + k^2l^2 + l^2h^2}{\left(h^2 + k^2 + l^2\right)^2}, \quad (4)$$

where h, k and l are the crystal plane indices. The diffraction elastic modulus decreased with increasing direction parameter Γ for the Reuss and the Kroener models, whereas the Voigt model gave a constant value independent of Γ.

The diffraction elastic constant for a specific crystal orientation can be read out from figure 13. For instance, $E_{210} = 140.0$ GPa and $E_{211} = E_{321} = 131.1$ GPa based on the Kroener model. In this figure, E_{ave} for $\Gamma = 0.2$ indicates the value averaged over all possible crystal orientations and corresponds to the macroscopic elastic modulus determined from the tensile test. For instance, E_{ave} was estimated as 136.0 GPa from the Kroener model (figure 13).

In bronze-processed Nb_3Sn strands, Nb filaments react with diffused-in Sn during the heat treatment and forms the Nb_3Sn compound. Due to the mechanism of compound formation, a layer of columnar Nb_3Sn grains grows around the filament and fine, equiaxed grains form in the filament core. Thus, the practical microstructure of the Nb_3Sn strand is not as simple and homogeneous as in the model structures discussed above. At least, the real value of the respective diffraction elastic modulus lies between the two extremes described by the Reuss and Voigt models.

In figures 6 and 7, the slope of the lattice strain as a function of applied strain for (210) tends to be smaller than those for (211) and (321). This phenomenon is attributed to the dependence of the elastic modulus on crystal orientation. As evidenced in figure 13, the elastic modulus for (210) is larger than that for the other crystal orientations.

4.4. Stress versus strain curve

As reported previously [16], stress versus strain curves can be evaluated on the basis of the rule of mixtures. Nb_3Sn strand includes five components (see the appendix). Stress on the strand is calculated by summing up the stress contribution from the constituent components as,

$$R_c = V_{f1}R_1 + V_{f2}R_2 + V_{f3}R_3 + V_{f4}R_4 + V_{f5}R_5, \quad (5)$$

where V_{fi} is the volume fraction of component i. For applied-strains up to 0.6%, it is presumed that Cu–Sn and Cu behave elasto-plastically, whereas Nb_3Sn and Nb behave elastically. The stress versus strain relation for each component is given by the following equations:

$$Nb_3Sn: R_1 = 1.36 \times 10^5 A \text{ (MPa)}, \quad (6)$$

$$Nb: R_2 = R_4 = (110 - 0.016T) \times 10^3 A \text{ (MPa)}, \quad (7)$$

$$Cu - Sn: R_3 = \frac{E_3 b_3 (A)^{1+1/n3}}{E_3 A + b_3 (A)^{1/n3}} \text{ (MPa)}, \quad (8)$$

$$Cu: R_5 = \frac{E_5 b_5 (A)^{1+1/n5}}{E_5 A + b_5 (A)^{1/n5}} \text{ (MPa)}, \quad (9)$$

where A is applied strain, T is temperature in kelvin, E_i is the elastic modulus of component i, and b_i and n_i are fitting parameters. Details for deriving the elasto-plastic expression given by equations (8) and (9) were provided in recent papers [6, 16].

Table 4. Diffraction elastic modulus and Poisson ratio at zero kelvin for Cu equiaxed poly-crystal calculated on the basis of the Kroener model, where Γ is the direction parameter.

hkl	Γ	E_{hkl} (GPa)	Poisson ratio
111	0.333	169.7	0.301
200	0	104.0	0.378
220	0.25	150.5	0.323
Average	0.2	139.8	0.336

Table 5. Parameters at 8.5 K for fitting the experimental data shown in figure 9 with equation (10).

hkl	E_{hkl} (GPa)	b_{hkl}	n_{hkl}
111	169.7	110	50
200	104.0	110	100
220	150.5	130	100
Average	139.8	117	84

The relation indicated in figure 9 of the lattice strain A_{hkl} as a function of applied strain A for the Cu component is given by the equation

$$A_{hkl} = \frac{R_{Cu}}{E_{hkl}} = \frac{b_{hkl}(A)^{1+1/nhkl}}{E_{hkl}A + b_{hkl}(A)^{1/nhkl}} \cdot 100(\%). \quad (10)$$

Diffraction elastic modulus with subscript *hkl* was evaluated according to the Kroener model and is listed together with the Poisson ratio in table 4. In this table, the average was calculated over all crystal orientations ($\Gamma = 0.2$). Hence, E_{ave} corresponds to the macroscopic elastic modulus, which can be measured by the tensile test.

We fitted the experimental data with equation (10) (as shown in figure 9) and used the diffraction elastic modulus listed in table 4. The fitting parameters b_{hkl} and n_{hkl} are listed in table 5.

According to the discussion above on micromechanics, parameters for calculating equations (8) and (9) are as follows: $E_3 = E_5 = E_{ave} = 139.8$ GPa, $b_3 = b_5 = b_{ave} = 117$ and $n_3 = n_5 = n_{ave} = 84$. The stress versus strain curve for the Nb_3Sn strand was calculated by equation (5) and is given by the solid curve $R_{Kroener}$ in figure 4. It fitted the experimental data quite well.

4.5. Load measurement at low temperature

Results of a similar experiment, conducted on a Nb_3Sn ITER wire with the same structure as the one studied herein, were reported in reference [6]. This earlier experiment was carried out by use of a different neutron facility installed at the atomic reactor and the thermal strain $A^T_{Nb_3Sn}$(axial) was estimated to be −0.16% and −0.099% at 9.3 K and room

temperature, respectively. The slope of $A^{\text{lattice}T}$ as a function applied strain was 1.34 for the axial direction from the single (321) diffraction peak and the force-free strain A_{ff} was estimated to 0.12% at 9.3 K [6]. Therefore, results in reference [6] show discrepancies compared with the present study.

In the earlier experiment [6], load was measured and controlled by a load cell installed outside of the evacuated load frame. Recently, it became clear that the load measured using this configuration was influenced by the evacuated load frame, which added a frictional load during cooling. As a result, it was very difficult to find exactly the zero-load level exerted on the wire sample. In contrast, in the present experiment, the zero-load level was correctly defined as the load where the wire sample fractured as shown in figure 3. Furthermore, to minimize errors, it is absolutely necessary to measure the sample load directly with a load cell that is placed within the evacuated load frame and connected in series with the sample as shown in figure 1. In this condition, the measured load more accurately represents the load applied on the sample at cryogenic temperatures. Hence, we recommend that the sample load be measured with the load cell installed within the evacuated load frame.

5. Summary

As a contribution to the international strain benchmarking activities, we measured the local strain exerted on Nb_3Sn filaments when subjected to longitudinal tensile strain. Using pulsed neutron technique, the change in crystal plane spacing generated by the application of strain was measured along the strand's axial and transverse directions at a temperature of 8.5 K. The lattice axial strain increased linearly with applied strain with a slope close to 1, while the lattice transverse strain decreased linearly with a slope of −0.33 to −0.34. The thermal axial strain was −0.22%. As a result, the force-free strain, which is a key parameter that determines the location of the peak of critical-current versus strain curve, was evaluated as to be 0.22–0.23% applied strain. Measurements of lattice strains on Nb and the Cu components revealed elastic and elasto-plastic behaviors of Nb and Cu components, respectively. Dependence of the diffraction elastic modulus on crystal orientation was calculated for Nb_3Sn based on micromechanics theories. The slope of lattice strain as a function of applied strain obtained from the diffraction peak of (210) was smaller than those from (211) and (321). This phenomenon related closely to the change of the diffraction elastic modulus with the crystal orientation. Parameters representing the elasto-plastic behavior of Cu were determined and used to calculate the stress versus strain curve for the ITER bronze-route Nb_3Sn strand investigated. The calculated curve described the measured macroscopic stress versus strain data quite well.

Table A1. Constituents of the Nb_3Sn strand and their volume fraction.

i	Component	V_f (%)
1	Nb_3Sn (filament)	11.2
2	Nb (core)	2.0
3	Bronze (matrix)	35.6
4	Nb (barrier)	1.7
5	Cu (stabilizer)	49.5

Acknowledgments

Author expresses his hearty thanks to Dr C Scheuerlein, CERN for his valuable suggestions. This work was supported in part by a grant-in-aid of the Ministry of Education, Culture, Sports, Science and Technology, Japan (26420669). The neutron diffraction experiments were performed at TAKUMI of S-PARC/MLF as the general research subject (Proposal No. 2013B0098). Bronze-route Nb_3Sn strand was provided by the ITER International Organization.

Appendix

Table A1 shows the constitution of the similar Nb_3Sn strand, which was fabricated by the same Japanese manufacturer.

References

[1] Ekin J W 1980 Strain scaling law for the flux pinning in practical superconductors: I. Basic relationship and application to Nb_3Sn conductors *Cryogenics* **20** 611
[2] ten Haken B, Godeke A and ten Kate H H J 1999 The strain dependence of the critical properties of Nb_3Sn conductors *J. Appl. Phys.* **85** 3247
[3] Markiewicz W D 2004 Invariant formulation of the strain dependence of the critical temperature Tc of Nb_3Sn in a three term approximation *Cryogenics* **44** 895
[4] Lu X F, Taylor D M J and Hampshire D P 2008 Critical current scaling laws for advanced Nb_3Sn superconducting strands for fusion applications with six free parameters *Supercond. Sci. Technol.* **21** 105016
[5] Arbelaez D, Godeke A and Prestemon S O 2009 An improved model for the strain dependence of the superconducting properties of Nb_3Sn *Supercond. Sci. Technol.* **22** 025005
[6] Harjos S, Ito T, Aizawa K, Arima H, Abe J, Moriai A, Iwahashi T and Kamiyama T 2011 Current status of engineering materials diffractometer at J-PARC *Mater. Sci. Forum* **681** 443–8
[7] Osamura K, Machiya S, Tsuchiya Y, Suzuki H, Shobu T, Sato M, Hemmi T, Nunoya Y and Ochiai S 2012 Local strain and its influence on mechanical-electromagnetic properties of twisted and untwisted ITER Nb_3Sn strands *Supercond. Sci. Technol.* **25** 054010
[8] Cheggour N, Nijhuis A, Krooshoop H J G, Lu X F, Splett J, Stauffer T C, Goodrich L F, Jewell M C, Devred A and Nabara Y 2012 *IEEE Trans. Appl. Supercond.* **22** 4805104
[9] Cheggour N *et al* 2015 International benchmarking of a selection of strain-measurement facilities available in the USA, Europe and Asia: first assessment at fixed temperature and magnetic field (unpublished)

[10] Jin X *et al* 2013 Development of a cryogenic load frame for the neutron diffractometer at Takumi in Japan proton-accelerator research complex *Rev. Sci. Instrum.* **84** 063106
[11] Moller H and Martin G 1939 Elastische Anisotropie und roentgenographisce Spannungs—messing *KWI-Eisenforsch* **21** 261–9
[12] Voigt W 1928 *Lehrbuch der Kristalphysik* (Leipzig: Teubner) p 962
[13] de Wit R 1997 Diffraction elastic constants of a cubic polycrystal *J. Appl. Crystallogr.* **30** 510–1
[14] Keller K R and Hanal J J 1966 Lattice softening in single crystal Nb_3Sn *Phys. Lett.* **21** 263–4
[15] Rehwald W, Rayl M, Cohen R W and Cody G D 1972 Elastic moduli and magnetic susceptibility of monocrystalline Nb_3Sn *Phys. Rev.* B **6** 363–71
[16] Osamura K *et al* 2013 Thermal strain exerted on superconductive filaments in practical Nb_3Sn and Nb_3Al strands *Supercond. Sci. Technol.* **26** 094001